

Article

Removal of Multiple-Radio-Frequency Interference in 1.29 GHz Wind Profiler Spectra

Kyung Hun Lee * and Byung Hyuk Kwon *

Major of Environmental Atmospheric Sciences, Division of Earth Environmental System Science, Pukyong National University, Busan 48513, Republic of Korea

* Correspondence: lee_buzz@nate.com (K.H.L.); bhkwon@pknu.ac.kr (B.H.K.)

Abstract: A 1.29 GHz wind profiler was developed under a private–military–government cooperative wind profiler radar development project in the Republic of Korea. During the test operation period, radio frequency interference (RFI) contamination occurred in the spectrum. In addition to the general shape, with a continuous appearance depending on the altitude, the spectrum showed complex shapes, such as discontinuous and overlapping frequencies. The RFI characteristics in the wind profiler spectra were analyzed, and a new algorithm was developed to remove multiple RFI (MRFI). Meteorological and non-meteorological signals were separated by filtering with a spectrum width threshold of 0.1 m/s. A continuity check was performed to determine MRFI in the non-meteorological signal. The number of gates in which the same radial velocity is continuous was determined based on whether the beam was vertical or oblique; a rough continuity test was performed, considering exceptional circumstances for the meteorological signal. For overlapping MRFI, the process was repeated. Spectral contamination by MRFI was removed through filtering and iterated scans; the continuity of wind vectors calculated from the improved spectral radial velocity was verified. Good-quality wind vectors can be produced even in a bad-radio-frequency environment if proper quality control is performed.

Keywords: wind profiler; multiple radio frequency interference; Doppler spectrum; radial velocity; spectrum width



Citation: Lee, K.H.; Kwon, B.H.

Removal of Multiple-Radio-Frequency Interference in 1.29 GHz Wind Profiler Spectra. *Atmosphere* **2023**, *14*, 1040. <https://doi.org/10.3390/atmos14061040>

Academic Editor: P.W. Chan

Received: 10 May 2023

Revised: 13 June 2023

Accepted: 14 June 2023

Published: 16 June 2023



Copyright: © 2023 by the authors. Licensee MDPI, Basel, Switzerland. This article is an open access article distributed under the terms and conditions of the Creative Commons Attribution (CC BY) license (<https://creativecommons.org/licenses/by/4.0/>).

1. Introduction

A wind profiler is a type of remote sensing equipment for observing the upper atmosphere. A pulse wave transmitted from the wind profiler to the atmosphere is backscattered into the atmosphere and returned, allowing the wind to be observed using the Doppler shift effect of the signal [1]. Wind is calculated using U (east-west wind) and V (north-south wind) measurements obtained via the IQ signal (In-Quadrature phase signal)–Doppler spectrum–spectral moment (doppler radial velocity) [2]. Wind profilers have been demonstrated to be more reliable than radiosondes and show excellent performance, which validates their accuracy [3]. However, the process of transmitting and receiving pulse waves and processing signals to observe wind can be hindered by various problems. These problems can be caused by hardware [4], surrounding terrain, buildings, wave-induced clutter [5–8], clutter caused by birds and aircraft [9,10], or contamination of the spectrum due to radio frequency interference (RFI) by the surrounding environment [11–13]. Spectral contamination by non-meteorological signals can make it difficult to find meteorological signals and decrease the accuracy of wind calculations. Therefore, like other remote observation equipment, such as synthetic aperture radar (SAR) satellites, wind profilers require quality control measures such as clutter removal and signal correction [14,15]. Thus, the detection and mitigation of RFI is an important topic in remote sensing research [16].

Previous wind profiler quality control studies have investigated various stages, including moment, spectrum, and IQ signal stages. Regarding the moment stage, statistical

processing of received power and spectrum width [17,18] and quality control using the spatiotemporal continuity homogeneity of radial velocity [19,20] have been investigated. For the spectrum stage, studies have focused on signal processing [21–23] and filtering techniques [24]. Moreover, regarding the IQ stage, wavelet transform of the time band has been investigated [25,26].

In the Republic of Korea, wind profilers have been used to observe upper winds and assimilate numerical model data [27]. However, since all current models have been made by foreign manufacturers, the aging of equipment and periodic equipment management are emerging as topics of concern. In cooperation with the Korea Meteorological Administration (KMA), Defense Acquisition Program Administration (DAPA), and private companies and universities, a private–military–government cooperative wind profiler radar development project was carried out for approximately four years from November 2017 to December 2021. From March 2021, during the test operation of the developed equipment at the Jeju National Typhoon Center (NTC) site, signal contamination due to RFI was observed multiple times. In addition to the generally known forms of RFI, multiple RFI (MRFI) was also observed; MRFI is discontinuous depending on altitude and is characterized by different frequencies overlapping several times. According to the National Oceanic and Atmospheric Administration (NOAA) [28], winds calculated from signals contaminated by RFI cannot be processed using quality control procedures such as consensus, which is a processing approach, as wind vectors appear as continuous and constant groups. The World Meteorological Organization recommends several frequency bands (50 MHz, 400 MHz, and 1 GHz) for avoiding RFI and for smooth wind observation [29]. However, this approach does not provide a clear solution to the interference caused by unlicensed frequency signals in the corresponding frequency band. Jordan et al. reduced the noise level through wavelet filtering in the time domain, a step before the Doppler spectrum, and removed intermittent interference using a harmonic wavelet filter [30]. Lambert et al. proposed the use of the vertical velocity threshold test, stating that the radial velocity of the oblique beam does not differ significantly in the presence of RFI and that the radial velocity of the vertical beam causes a very large feature [18,31]. The National Center for Atmospheric Research (NCAR) proposed a statistical technique, which is based on the weight of each variable, using various variables such as spectral moment and asymmetry to identify and remove RFI [32]. Since then, numerous studies have investigated this topic using fuzzy logic [23,33,34]. Sinha et al. presented a method for detecting RFI according to fluctuations in power spectral density (PSD) and range and Doppler bins [35].

Until recently, the proposed RFI removal methods have focused on general RFI; hence, they cannot be applied to the MRFI that appeared during the test operation. Therefore, it is necessary to develop an individual algorithm for MRFI removal. We developed an algorithm that identifies the characteristics of MRFI and removes them at the spectrum stage, allowing real-time quality control to be automatically performed in the field. After applying the algorithm, MRFI no longer appeared in the spectrum.

The paper is organized as follows. Section 2 introduces the test equipment, data, and observatories used to develop MRFI removal algorithms and presents the process of developing a removal algorithm for MRFI. The results of applying the MRFI removal algorithm under various cases and the applicability of the algorithm are presented in Section 3. Sections 4 and 5 present the discussion and conclusion of the study, respectively.

2. Materials and Methods

2.1. Equipment

The wind profiler used in this study uses a frequency of 1.29 GHz and an active phased array antenna to freely observe the wind in the air without limiting the azimuth. It was developed to be observable from 0.15–12.0 km with a vertical resolution of 50–100 m every 10 min. The wind profiler can be installed and used for observations at a fixed location. Additionally, it can be mounted on a vehicle and used as a mobile device, allowing more

convenient observation of the wind and securing of data. Detailed specifications are given in Table 1.

Table 1. Specifications of the wind profiler.

Parameter	Specification
Operation frequency	1.29 GHz
Antenna type	Active phased array
Peak power	>1.8 kW
Pulse width	0.333–10.8 μ s
Minimum height	150 m (dependent on pulse width, meteorological conditions, environment)
Maximum height	12 km (dependent on pulse width, meteorological conditions, environment)
Height resolution	50 m, 100 m (dependent on pulse width)
Horizontal wind speed detectable range	\pm 50 m/s
Vertical wind speed detectable range	\pm 20 m/s
Wind speed accuracy	RMSE < 1.0 m/s
Wind direction accuracy	RMSE < 10.0°
Time resolution	10 min
The number of FFT (fast Fourier transform) points	1024

2.2. Data

We used raw spectral data and raw moment (radial velocity, spectrum width, noise [36]) data produced during the test operation period (March–April 2021). The raw spectral data was used to analyze the various non-meteorological signals that appeared in the spectra, and the raw moment data was used to compare the pre-quality-control winds to the post-quality-control winds.

2.3. Site

The test bed was located on the large site of NTC on Jeju Island, an island off the southern coast of the Republic of Korea (see Figure 1). Jeju Island is a volcanic island with Mt. Halla, which has an elevation of approximately 2 km, located at the center of the island. The island shows different meteorological characteristics from east to west and north to south due to topographic effects [37]. The island was chosen to test the wind profiler as it is also famous for its windy climate and relatively large amount of water vapor observed throughout the year.

Prior to constructing the test bed, an assessment of the radio frequency environment was conducted. Incoming radio frequencies within the 1.26–1.32 GHz frequency band of the development equipment were not observed (see Figure 2). The frequency range was subsequently extended to 1.0–6.0 GHz, following which a total of 12 incoming radio signals of unknown purpose were identified (see Figure 3). Detailed information on the incoming radio signals is given in Table 2. In general, it is known that radio signals of the same frequency cause interference [38]. However, according to ISO/DIS 23032 [39], even if the interfering frequency is different from the wind profiler frequency, interference contamination can occur in the baseband due to processes such as receiver modulation and aliasing of the sampling frequency. Therefore, it can be surmised that the RFI contamination observed during the test operation was caused by radio signals in the 1.333 GHz frequency band within the baseband (\pm 60 MHz) range of the development equipment.

2.4. Multiple Radio Frequency Interference

MRFI refers to the phenomenon when the peaks at a single frequency are discontinuous with altitude, or when the peaks at several frequencies are continuous with altitude (Type A), which gives the appearance of a single RFI but is actually an overlap of multiple frequencies (Type B). Interference signals of multiple frequency bands appear in radars of

ultra-wide bands ranging from less than 100 MHz to several GHz, but irrespective of the large amount of RFI that has been reported in literature, they have not been documented with regard to wind profilers [40]. Figure 4 shows an example of a Type A MRFI spectrum obtained during the test. In the beam, it can be seen that radio interference peaks appear continuously in all directions with altitudes at around -100 FFT (approximately 0 to 2.0 km) and around -450 FFT (approximately 2.0 to 12.0 km). This demonstrates peaks at several frequencies of Type A that are continuous with altitude.

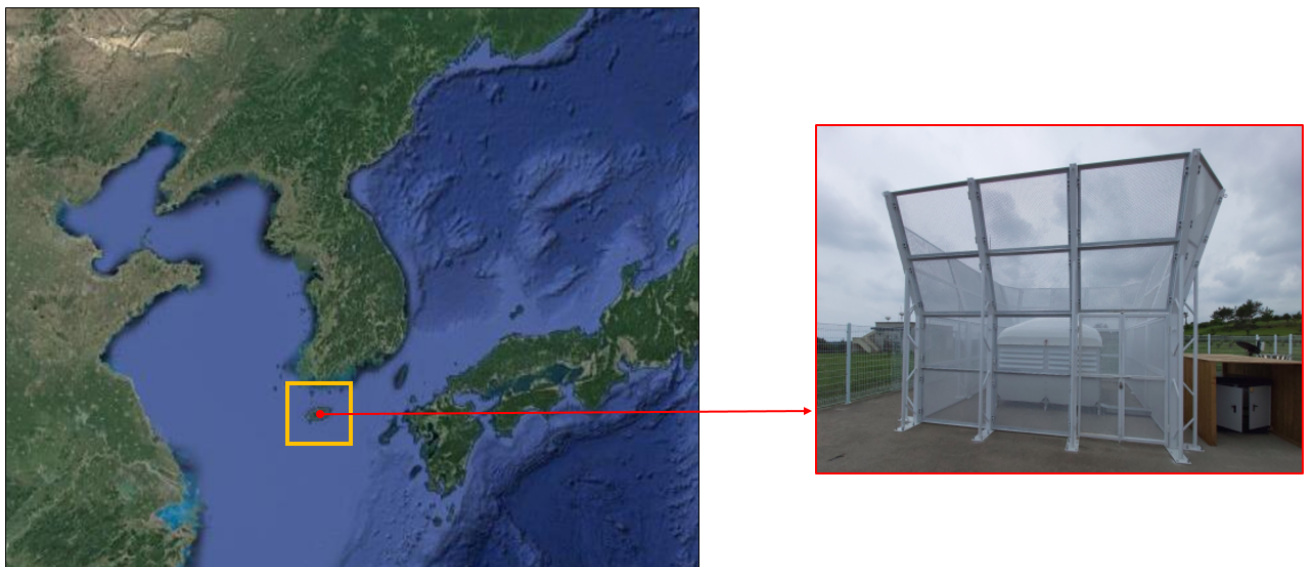


Figure 1. Wind profiler testbed, located at the National Typhoon Center on Jeju Island, south of the Korean peninsula, © Google Maps.

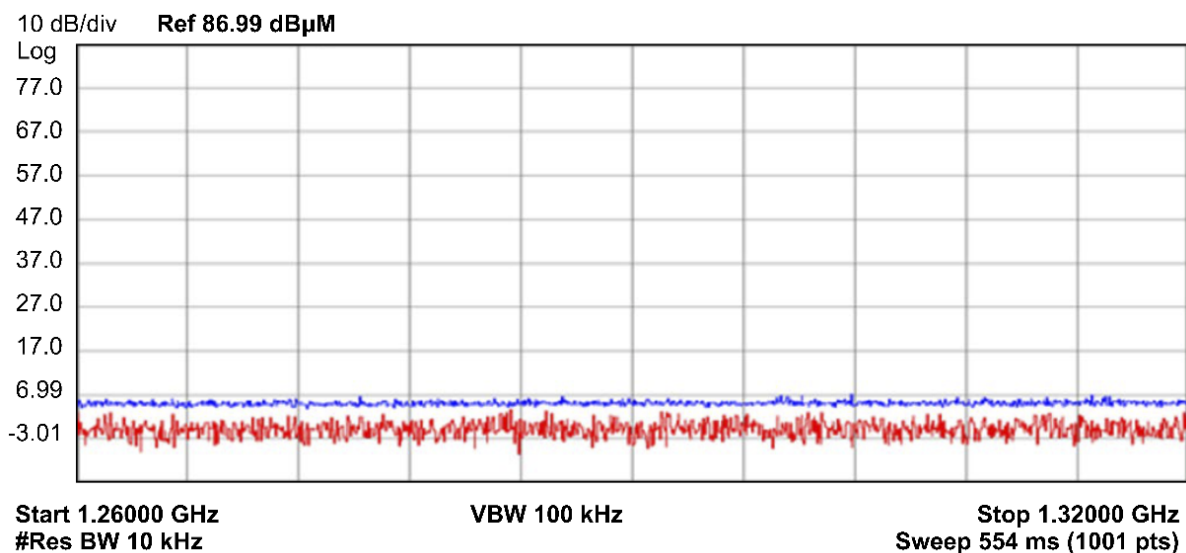


Figure 2. Radio signal test between 1.26 and 1.32 GHz at the testbed on 15 September 2020. The abscissa is the frequency (GHz), and the ordinate represents the logarithmic signal power in $\text{dB}\mu\text{V}/\text{m}$. The blue line shows the peaks that occur occasionally, while the red line was filtered to remove harmonics and show only the continuous peaks. Radio signal from 1.26 GHz to 1.32 GHz were not detected.

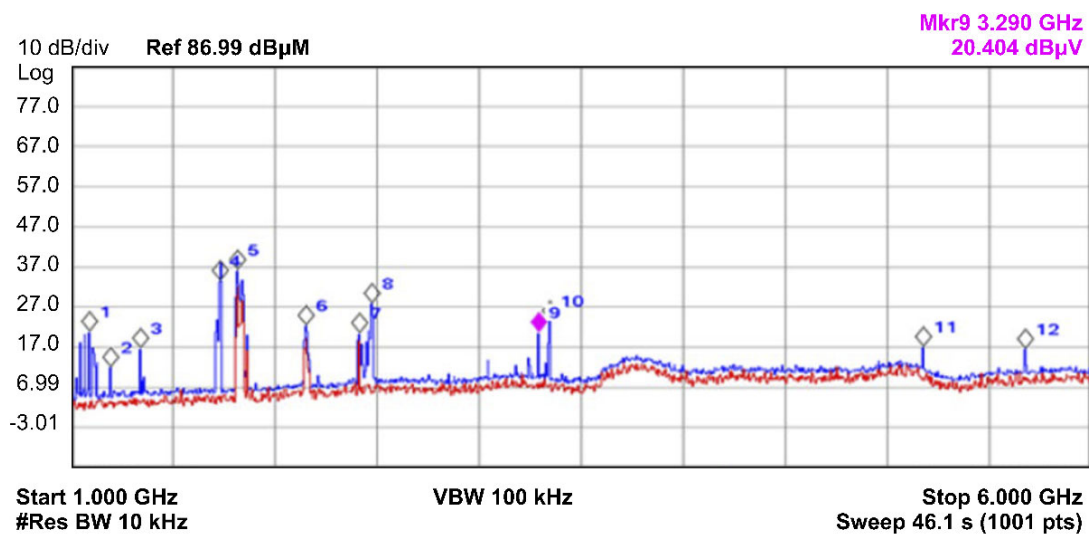


Figure 3. Same as Figure 2 but for a signal test range of 1 to 6 GHz. Twelve radio signals were detected. The details of the 12 radio signals are shown in Table 2.

Table 2. Details of the radio signals received in the testbed.

Number	Frequency (GHz)	Signal Power	
		(db μ V/m)	(dBm)
1	1.090	20.00	−86.4
2	1.195	11.83	−95.2
3	1.333	16.48	−90.5
4	1.730	33.29	−73.7
5	1.815	35.98	−71.0
6	2.150	22.11	−84.9
7	2.415	20.21	−86.8
8	2.475	27.69	−79.3
9	3.290	20.40	−86.6
10	3.354	23.35	−86.6
11	5.175	16.81	−90.2
12	5.675	16.39	−90.6

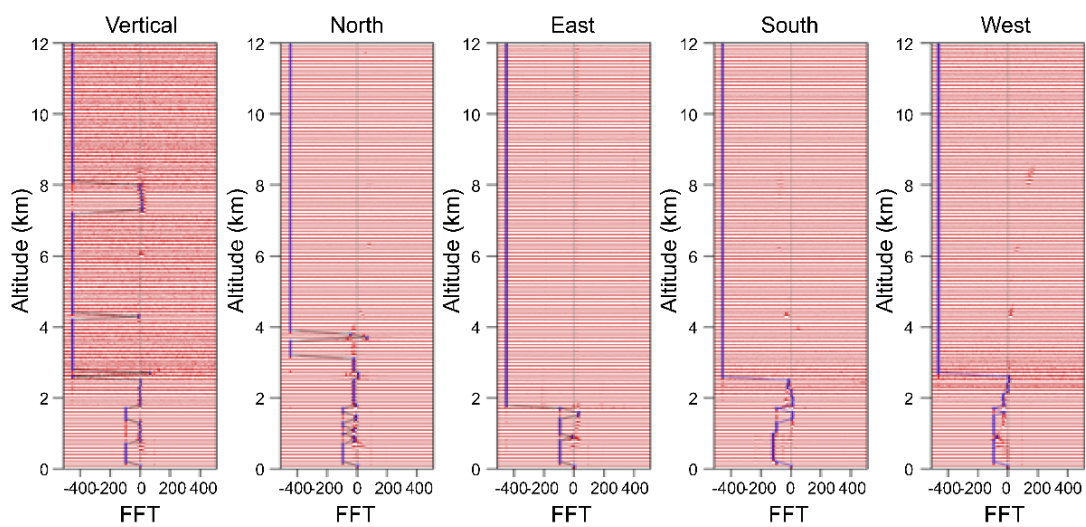


Figure 4. A Type A MRFI detected at 10:37 KST on 9 April. Spectral peaks (blue) are plotted above the normalized spectral power density (red).

Figure 5a shows an example of the Type B MRFI spectrum that appeared at the time of the test. Subsequently, the interference contamination was removed manually, and the result is shown in Figure 5b to Figure 5d. In Figure 5a, it can be seen that continuous peaks appear at approximately 2.0 to 12.0 km around 400 FFT. When the corresponding peak was first removed, radio interference reappeared at approximately 2.0 to 12.0 km around -400 FFT, as shown in Figure 5b. In Figure 5c, with the corresponding peak removed again, it can be seen that the polluted peak near -400 FFT was removed, and the weather signal appeared at an altitude of 3.5 to 6.0 km. When the remaining interference contamination at 2.0 to 3.5 km and 8.0 to 12.0 km was removed, some meteorological signals between 2.0 to 3.5 km were restored. Finally, the meteorological signals were restored up to 0.5 to 6 km (Figure 5d). In Figure 5a, the peak at 0 to 300 m was assumed to be RFI, but it is not at the same frequency as the interference signal at 2.0 to 12.0 km, and is 3-gate; hence, it was not removed. These findings confirm that the meteorological signal can be restored through iterative removal, even if the RFI hidden in the RFI with the greatest spectral power is small.

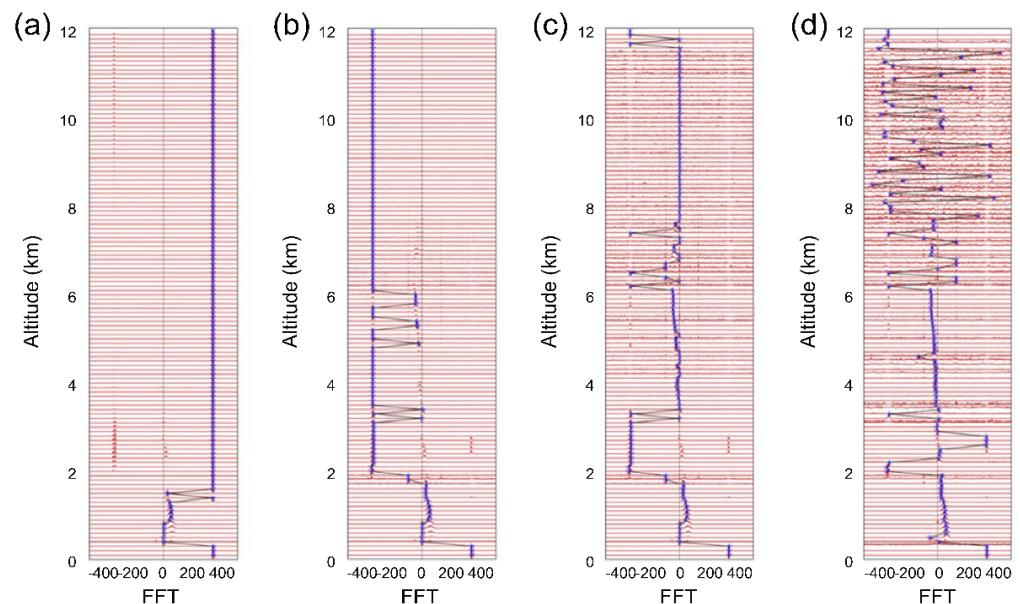


Figure 5. Type A MRFI on the east beam, detected at 10:16 KST on 1 April: (a) raw spectra, (b) spectra after the first manual removal of MRFI from the raw spectra, (c) spectra after a second manual removal of MRFI from the raw spectra, and (d) spectra after a third manual removal of MRFI from the raw spectra. Spectral peaks (blue) are plotted above the normalized spectral power density (red).

2.5. MRFI Removal Algorithm

RFI degrades the quality of wind vectors, impairing the testing and operation of wind profilers [41]. The best practice is to conduct observations in a good environment free of RFI; as this is not always possible, it is necessary for wind profilers to be able to operate in a poor environment [11]. However, it is difficult to manually identify and remove the occurrence of MRFI. Therefore, an algorithm was developed to automatically identify and remove MRFI from the raw spectrum stage.

A spectral peak signal contaminated by RFI has characteristics similar to noise signals among non-meteorological signals. Therefore, to check for RFI contamination, the process of distinguishing meteorological signals from non-meteorological signals was performed first. Spectrum width testing is mainly used as a method for distinguishing meteorological and non-meteorological signals in the spectrum stage [42]. The spectrum width of a non-meteorological signal is generally known to be less than 0.2 m/s for noise signals and more than 4 m/s for signals caused by non-meteorological objects such as birds or aircraft. In

particular, signals caused by RFI appear as very narrow spike-shaped peaks, which are characterized by a small spectrum width [28].

Figure 6 shows a histogram of 7647 spectrum widths from the observation data for March 2021. Most of them are distributed within 2 m/s, and noise signals mostly occur below 0.1 m/s. Approximately 25% of the spectrum widths were above 0.1 m/s, and approximately 75% were below 0.1 m/s, which is similar to the percentage of noise that makes up most of the signals, except for some meteorological signals. Therefore, filtering was performed with a spectrum width threshold of 0.1 m/s. Figure 7 shows an example of external RFI, and peaks with a spectrum width of 0.1 m/s or more among the peaks for each gate are displayed in green. The green peak at an altitude of 0 to 3.5 km is a precipitation signal (blue box); the vertical beam has a large radial velocity, and the oblique beam is positively deflected. Moreover, a rainfall intensity of approximately 8 mm/h was confirmed with a test bed rain gauge. At an altitude of 3.5 to 6.0 km, wind signals were detected (sky-blue box). The north and south beams are symmetrical, as well as the east and west beams. The noise signal was not shown, indicating that the spectrum width threshold filtering was well-applied.

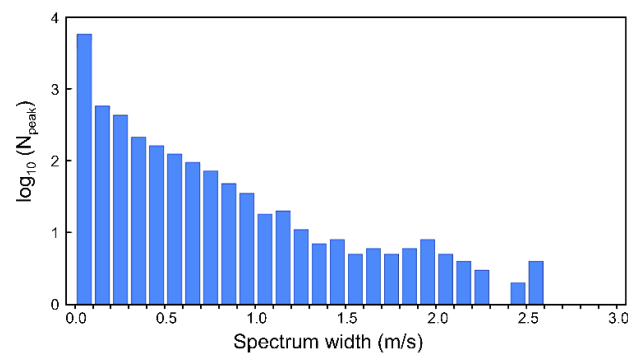


Figure 6. Distribution of spectrum width for 31 days. The scale of the bar indicates the logarithmic number of spectrum widths in the same range.

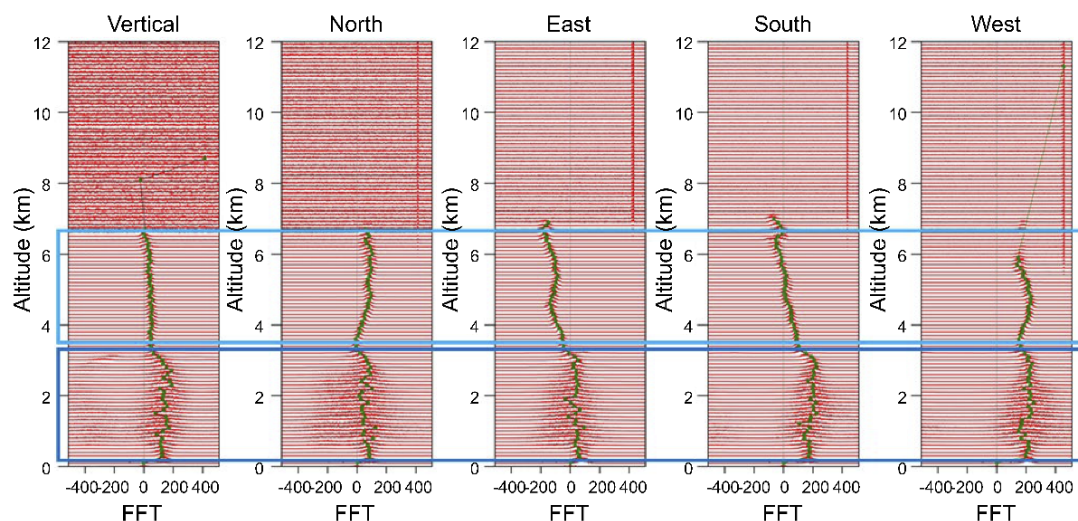


Figure 7. Spectral peaks (green) higher than a threshold of 0.1 m/s, measured at 15:22 KST on April 12 are plotted above the normalized spectral power density (red). Blue and sky-blue boxes show rainfall and wind signal, respectively.

After applying spectrum width threshold filtering, a continuity check was executed on the identified gate, which was suspected of being a noise signal, in order to confirm potential contamination by RFI. To retrieve Type A MRFI, the continuity criterion was set as four or more contaminated gates in the same FFT at all altitudes. To identify discontinuous

peaks by altitude, the standard was set between three gates (300 m based on this equipment), which is a general vertical wind shear check standard [42], and 1.0 km, following which the RFI retrieval performance was tested. Based on MRFI contamination cases, 400 m (approximately 1/8 of the number of low-mode gates) was set as the standard. If the continuity check revealed MRFI contamination, 5 points (± 2 points) from the corresponding peak were subjected to noise-ization (Equation (1)) to remove MRFI, and a new peak was derived. Noise-ization is used to completely remove MRFI and avoid the problem of the linear interpolation method in which the contaminated peak remains even though the peak is removed. Noise-ization was applied following Equation (1):

$$f(n) = \frac{S\left(\frac{FFTn}{2}\right) + S\left(\frac{FFTn}{2} + 1\right)}{2}, \tag{1}$$

where n is the number of points in the range 1–5, and $f(n)$ is the power spectral density of points. $FFTn$ is the number of FFT , and $S(n)$ is the sorted power spectral density of points.

A continuity check was also performed on gates determined to be meteorological signals in preparation for non-meteorological signals that the spectrum width threshold filtering did not filter out. This is to avoid diminishing the performance of the algorithm due to infrequent problems. However, to prevent the actual meteorological signal from being removed, the continuity criterion was set to 15 or more gates for vertical beams and 8 or more gates for oblique beams (approximately 1/2 and 1/4 of the total gates, respectively, based on the number of gates in low mode). Next, linear interpolation (Equation (2)) of five points of the corresponding peak was performed. Linear interpolation is intended to maintain some of the peak shape of the signal after removal. An example of noise-ization and linear interpolation is shown in Figure 8. Linear interpolation followed Equation (2):

$$f(n) = \left(1 - \frac{n - 1}{P_5 - P_1}\right) \times f(1) + \left(\frac{n - 1}{P_5 - P_1}\right) \times f(5) \tag{2}$$

where n is the number of points in the range 2–4.

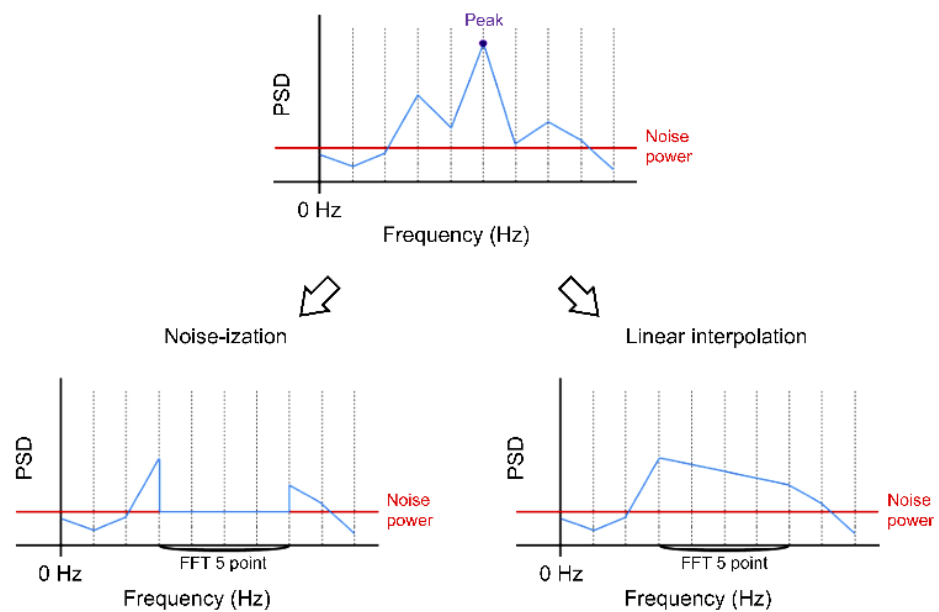


Figure 8. Schematic diagram for noise-ization and linear interpolation of MRFI.

2.6. Repeat Scanning

To remove the double and triple overlapping Type B MRFI, the removal process was repeated until the continuity was below the criterion point. Spectrum width [43] was calculated for the newly derived peak in the iterative process, and filtering, using this as a

threshold value, and the continuity check were performed again (see Figure 9, Equation (3)). Spectrum width was calculated according to Equation (3):

$$\sigma_w = \sqrt{\left(\frac{\sum_i^n S_i \times (v_i - v_r)^2 \times \Delta f}{P_r}\right)} \tag{3}$$

where n is the number of peak FFT points.

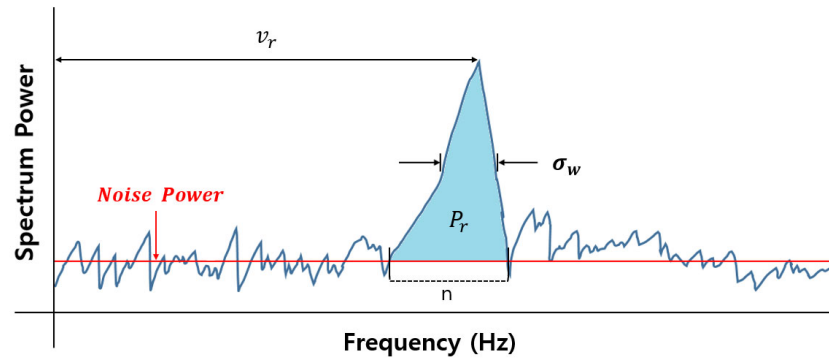


Figure 9. Schematic diagram of the Doppler spectral moment calculation.

Considering this iterative process, it is important to establish an appropriate continuity criterion point. The schematic diagram of the algorithm of the MRFI removal process is shown in Figure 10.

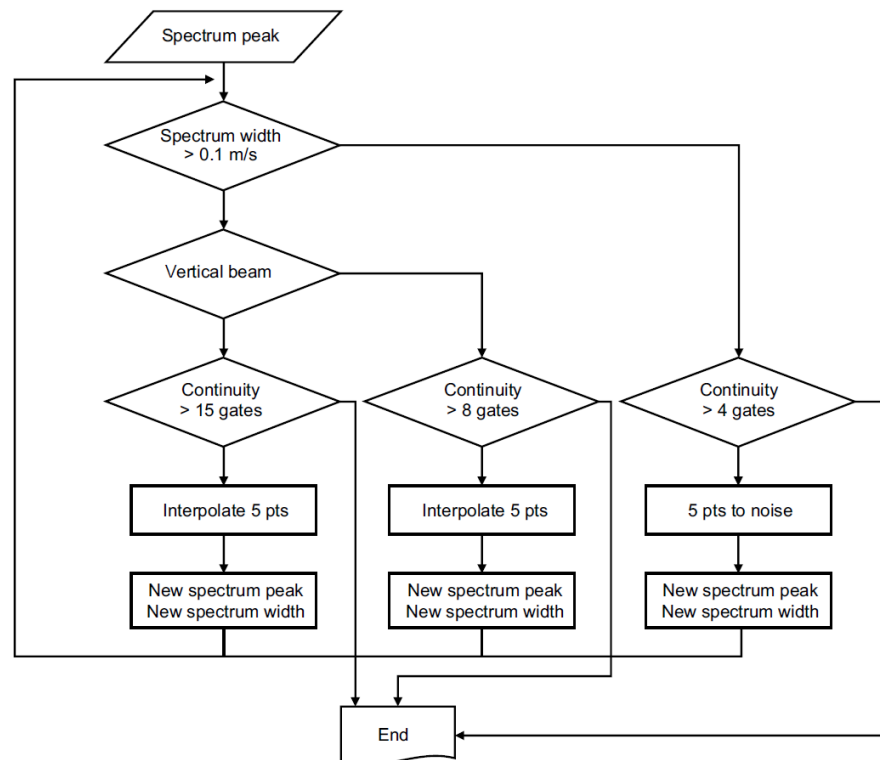


Figure 10. Flow chart for removal of MRFI. For peaks with spectrum widths less than 0.1 m/s, continuity is evaluated by altitude, and if continuous, it is denoised to find new peaks and calculate their spectrum width. The same process is performed for weather signals with spectrum widths greater than 0.1 m/s, with the only difference being the threshold, and the process is repeated until all pass the continuity evaluation.

3. Results

To confirm the usefulness of the MRFI removal algorithm, we performed a comparative analysis by calculating the spectrum and wind vector before and after the MRFI removal. The results are discussed in the subsequent sections. The wind vector was calculated using the doppler beam swinging (DBS) method using the radial velocity obtained by the moment method.

3.1. MRFI Cases

During the analysis period in April 2021, 12 MRFI were identified (see Table 3). Most tended to be concentrated during a specific time (morning) and on specific days (two, six, and four times on 1, 9, and 13 April, respectively). The south beam had the least number of MRFI with two occurrences, followed by the east, west, vertical, and north beams with four, four, six, and seven occurrences, respectively. In addition, half of the cases occurred simultaneously with beams in several directions instead of in one direction. With regard to mode, cases occurred more frequently in high mode than in low mode. As for the types, Type A and B were observed seven and four times, respectively, with both types appearing at the same time once. Herein, 4 out of 12 cases of MRFI have been discussed. These four cases were selected on the basis of distinct days, different observation modes, different types, and clear MRFI.

Table 3. MRFI cases.

Case	Date (KST)	Mode	Contaminated Beam					RFI Type
1	1st April 10:16:25	High		East				B
2	1st April 10:57:38	High				West		A
3	9th April 10:13:09	High	Vertical					A, B
4	9th April 10:37:02	High	Vertical	North	East	South	West	A
5	9th April 10:49:05	High	Vertical	North				A
6	9th April 11:22:21	High	Vertical					A
7	9th April 12:01:15	High	Vertical	North	East	South	West	A
8	9th April 12:24:43	High		North				A
9	13th April 10:14:56	High		North				A
10	13th April 11:38:25	High	Vertical					B
11	13th April 11:44:14	Low		North			West	B
12	13th April 11:55:55	Low		North	East			B

3.1.1. Case 2

On 1 April 2021, at 10:57 KST, Type A MRFI was observed in the high-mode west beam. Short altitude-spaced peaks appeared across all altitudes at around -300 FFT and around 400 FFT (Figure 11a). The interference-contaminated peak was identified as a noise signal (Figure 11a; purple box) by spectrum width filtering. MRFI appearing at such a short altitude interval is difficult to retrieve and remove; however, the MRFI removal algorithm was able to eliminate most of the contaminated peaks that appeared near -300 FFT and 400 FFT. Figure 11 shows that the meteorological signal (green) was restored at approximately 4.0 to 9.5 km.

3.1.2. Case 3

On 9 April 2021, at 10:13 KST, MRFI occurred in a high-mode vertical beam. In the spectrum produced before MRFI removal, continuous interference peaks at each altitude appeared around -100 and 400 FFT, considered to be Type A (Figure 12a). There were also traces of RFI near 450 FFT that were removed, indicating that Type A and Type B coexist in the spectrum after MRFI removal (Figure 12b). Figure 12b shows that the meteorological signal is restored at an altitude of approximately 0.5 to 8.5 km. It is also well suited to the meteorological signature of a vertical beam with a peak near 0 FFT (0 m/s).

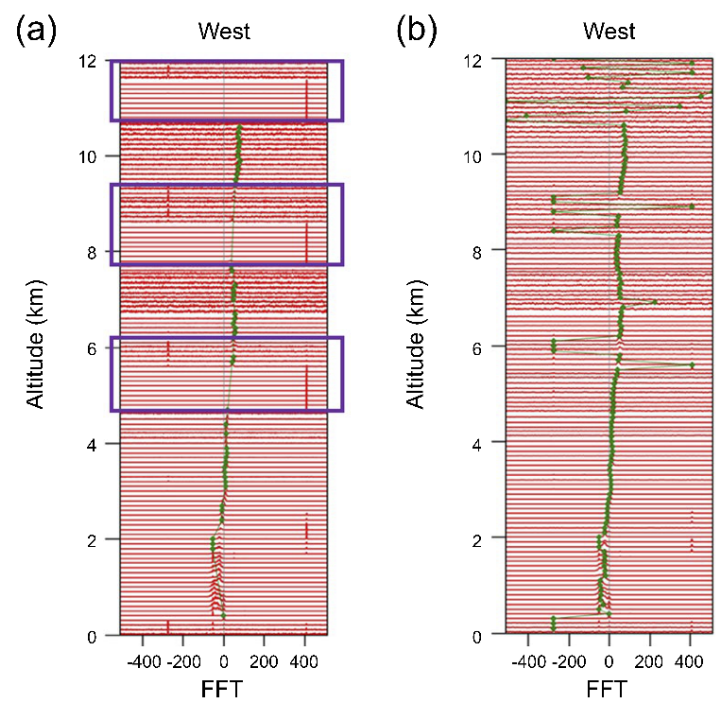


Figure 11. (a) Raw spectra and (b) quality-controlled spectra obtained using the removal algorithm. Spectral peaks (green) higher than a threshold of 0.1 m/s, measured at 10:57 KST on 1 April are plotted above the normalized spectral power density (red). The purple box indicates the signals considered as the MRFI.

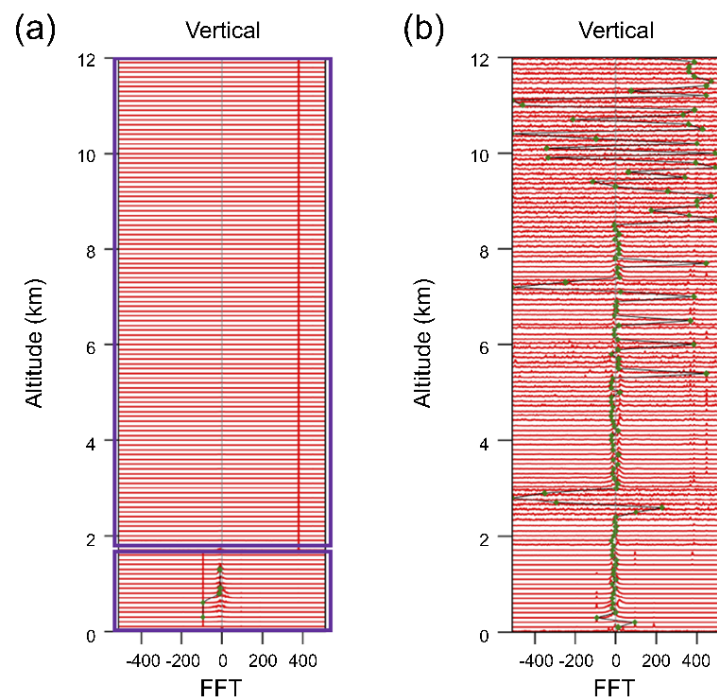


Figure 12. Same as Figure 11 but obtained at 10:13 KST on 9 April.

3.1.3. Case 11

On 13 April 2021, at 11:44 KST, Type B MRFI occurred in low-mode north beam and west beam. For both beams, continuous interference peaks around 200 FFT appeared, up to 0.7 to 3.5 km altitude (Figure 13). Spectrum width filtering confirmed that the peak was a noise signal (purple box). In Figure 14, after MRFI was removed, it can be seen that, in

addition to the peak near 200 FFT, which was first seen in the north beam, RFI overlapped through the remaining traces at 2.0 to 3.5 km near 300 FFT. Moreover, the meteorological signal was well restored at 0.7 to 3.5 km altitude in both beams.

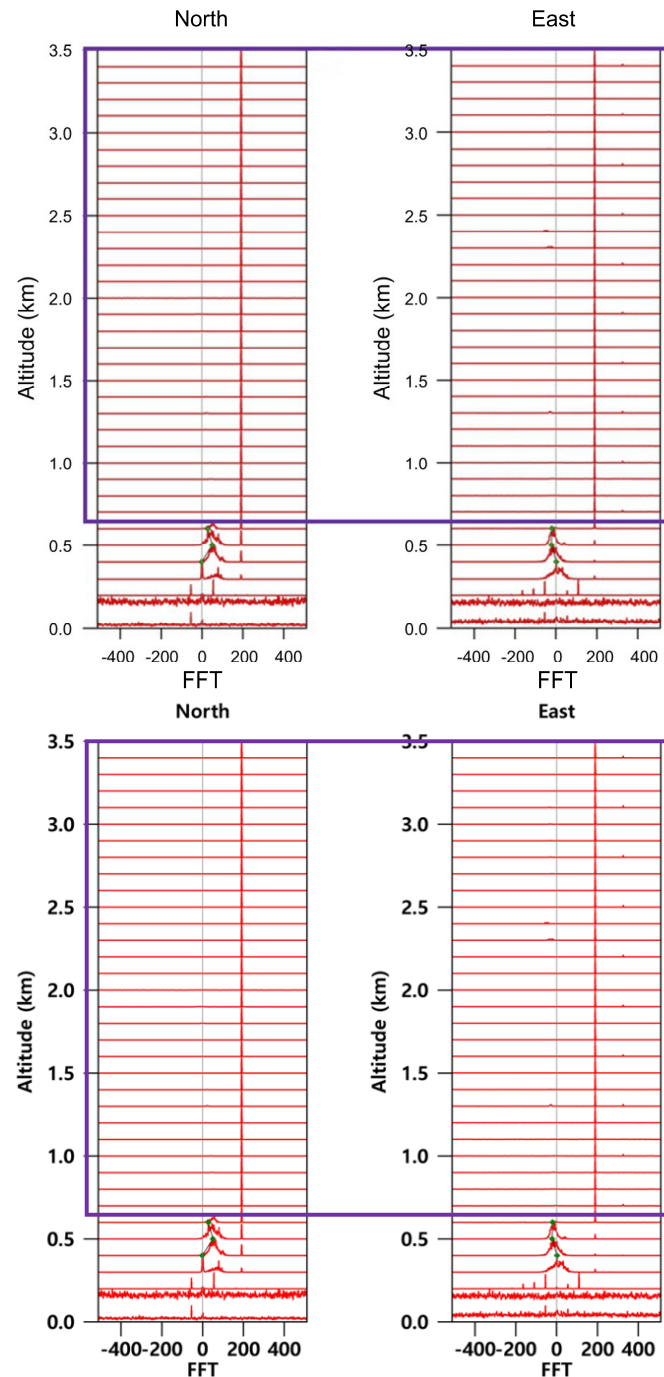


Figure 13. Raw spectra measured at 11:44 KST on 13 April. Spectral peaks (green) higher than a threshold of 0.1 m/s were plotted above the normalized spectral power density (red). The purple box indicates the signals identified as the MRFI.

3.1.4. Case 12

In Case 12, Type B MRFI contamination occurred in the low-mode north beam and east beam at 11:55 KST on 13 April 2021. Similar to Case 11, a continuous interference peak appeared near 200 FFT. This was identified as a noise signal due to filtering (purple box) (Figure 15). The east beams in Figures 15 and 16 show that, in addition to the 200 FFT,

there was a continuous interfering signal that overlapped near 300 and 450 FFT. MRFI was completely removed after the algorithm was applied, and the meteorological signal was restored up to approximately 0.3–3.5 km (Figure 16).

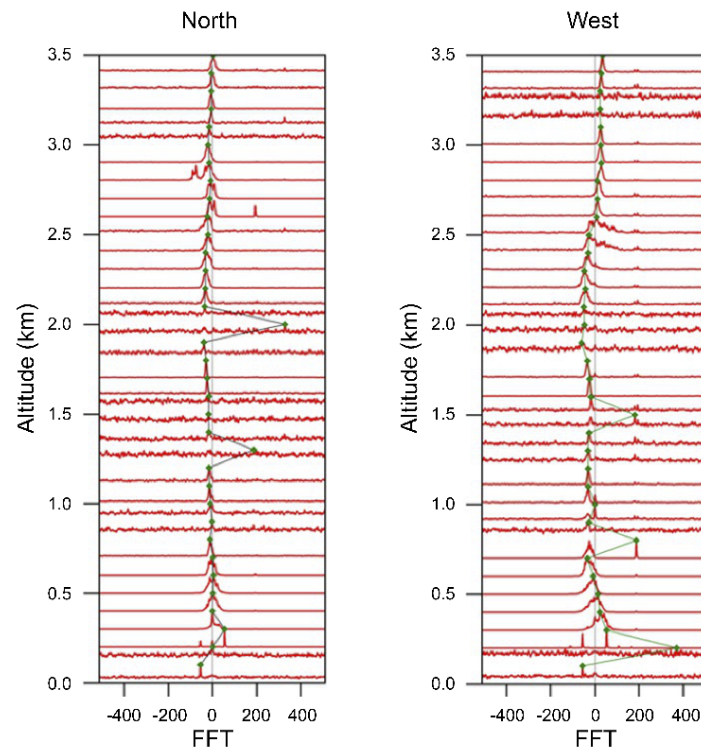


Figure 14. Quality-controlled spectra produced using the removal algorithm. Spectral peaks (green) higher than a threshold of 0.1 m/s were plotted above the normalized spectral power density (red).

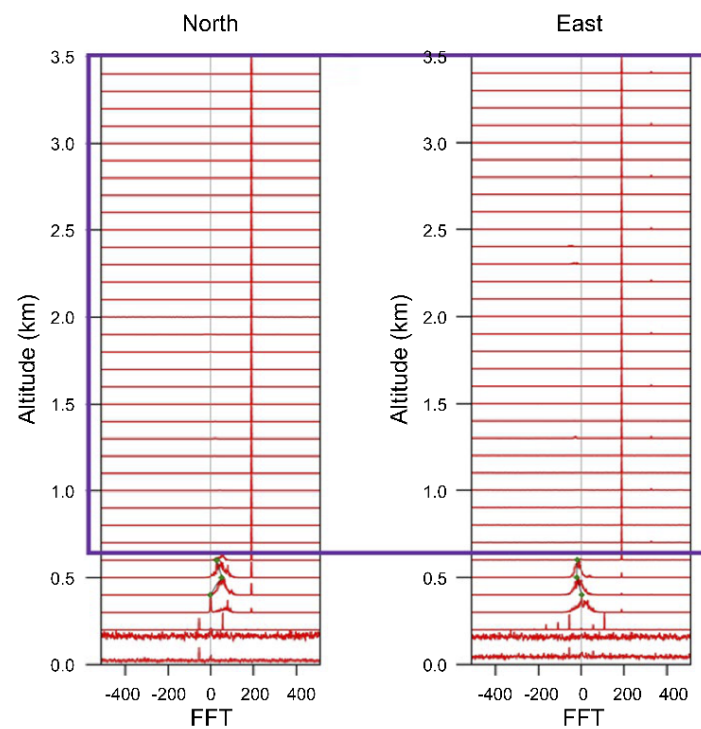


Figure 15. Same as Figure 13 but obtained at 11:55 KST on 13 April.

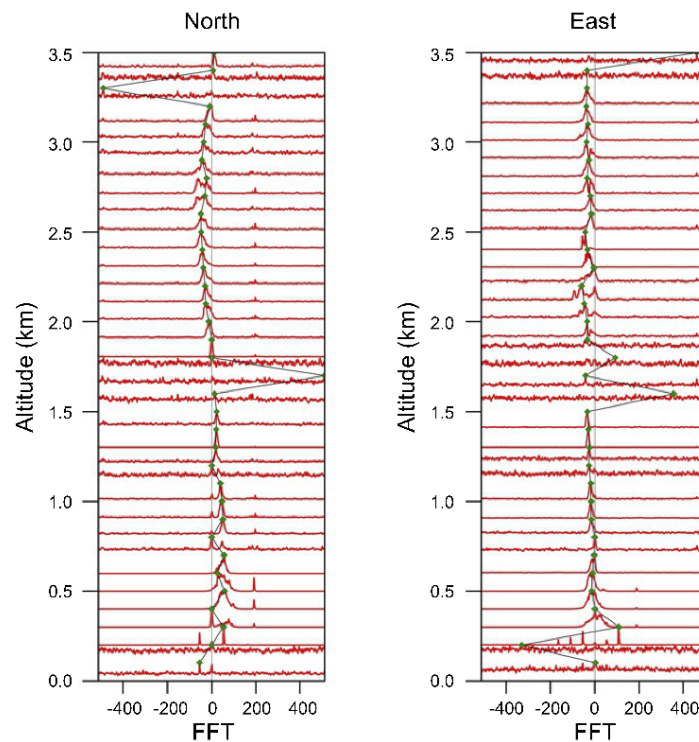


Figure 16. Same as Figure 14 but obtained at 11:55 KST on 13 April.

The horizontal wind vector during 13 April 2021, when RFI was significant, is shown in the time series (Figure 17). At 09:45 and 10:20, discontinuous wind vectors due to RFI were observed. Moreover, at 11:44 (Case 11) and 11:55 (Case 12), strong northwesterly and northeasterly winds appeared uniformly along the altitude, similar to MRFI that appeared on the north-west beam and north-east beam in spectra.

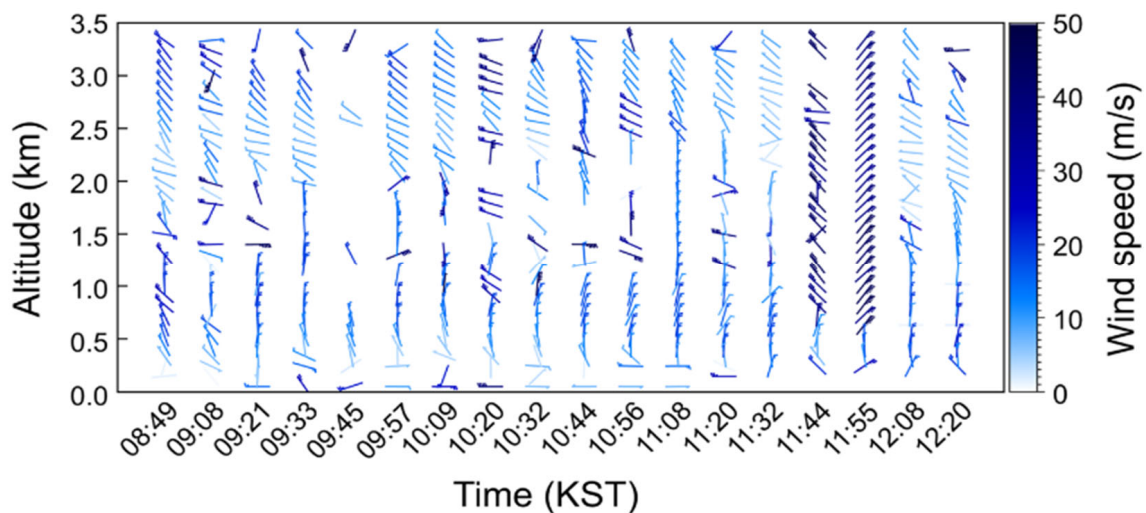


Figure 17. Wind vector field produced with raw spectra on 13 April.

The horizontal wind vector time series, to which the MRFI removal algorithm was applied, shows that the discontinuous wind vectors were removed and that the wind vectors were continuous in space and time (Figure 18). Additionally, at 11:44 and 11:55, the temporally continuous wind vectors of the north wind in the lower layer and the west wind series in the upper layer appear. Therefore, the correct meteorological signal was restored by removing MRFI.

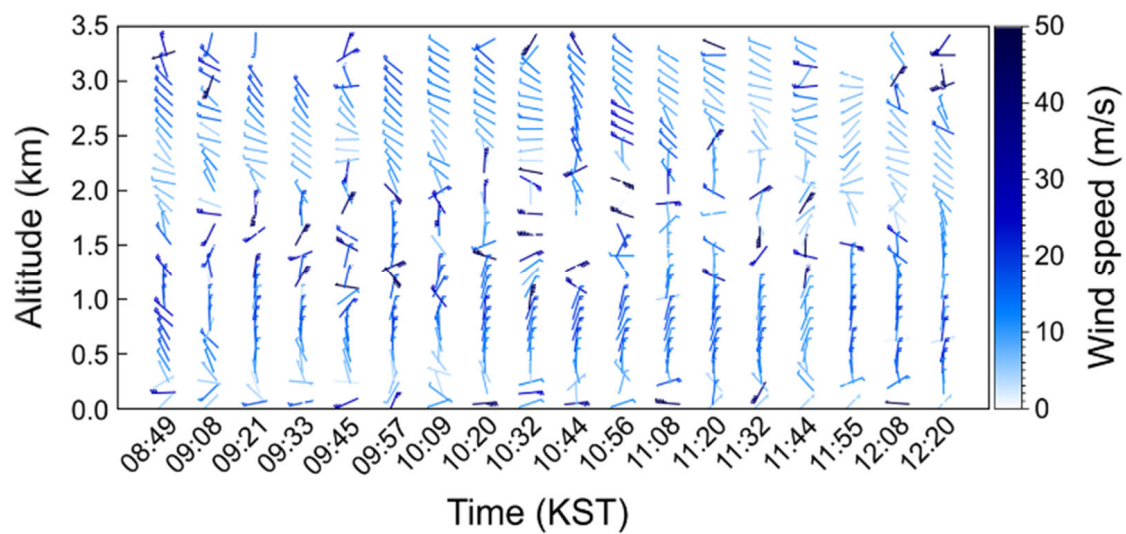


Figure 18. Wind vector field produced with quality-controlled spectra obtained using the nova algorithm to remove MRFI on 13 April.

4. Discussion

Previous studies have presented methodologies for RFI removal at the IQ signal level or the Doppler spectrum level. Both types of methods have key strengths and weaknesses; however, the present study was conducted at the Doppler spectrum stage for ease of data acquisition during the equipment development process and for the convenience of future research (researchers can clearly view the series of processes applied for the generation and removal of RFI).

The MRFI mentioned in the present study has the RFI characteristics mentioned in the introduction, and the removal process is more complex than that of RFI. There are two key challenges with MRFI removal at the Doppler spectral level. First, it is difficult to pinpoint the frequency at which RFI occurs. Since RFI has a large environmental factor, it is difficult to accurately identify which frequency peak on the spectrum represents RFI. In the case of MRFI, this is more challenging due to the difficulty of visually checking due to overlapping, as shown in Figure 5. Second, it is difficult to set a continuity threshold. Generally, peaks emerge consecutively over 1 km on the spectrum [31]; however, this can vary depending on several factors. In particular, it is difficult to determine the continuity threshold because it emerges briefly in some cases, as shown in Figure 11a when MRFI occurs.

Therefore, considering the above challenges, we focused on identifying the MRFI characteristics and seeking strategies to address them. Spectrum width filtering, altitude continuity evaluation, and FFT point removal methods introduced as MRFI removal methods are commonly used for quality control. We attempted to implement an algorithm by introducing these methods to meteorological signal discrimination, RFI discrimination, and RFI removal and setting appropriate threshold values (Section 2.5). As shown in Figures 6 and 7, the spectrum width filtering works well, and the set threshold of 0.1 m/s is appropriate, which was also satisfactory in other manufacturers' models (PCL-1300, LAP-3000, LAP-8000, CLC-11-H, CFL-03). Altitude continuity thresholds may vary depending on the number of gate spacings and gates, as well as the maximum observation altitude. Therefore, they are influenced by pulse width, pulse repetition time, and sampling frequency. Five-point FFT is also a commonly used method, but it can change depending on the number of FFT points and the frequency resolution (radial velocity resolution). It does not matter if the threshold (0.3 m/s to 1 m/s) is set by converting the FFT points to radial velocity.

Among the 12 MRFI cases, the four selected cases adequately represent the challenges we mentioned above. In all four cases (Figures 11a, 12a, 13 and 15), MRFI characteristics are exhibited well, including continuous peaks at different frequencies and continuous peaks

of short altitude intervals in the raw spectrum. The meteorological signal is restored well even after application of the MRFI removal algorithm. The effect of MRFI on the horizontal wind vector calculation can be observed clearly in Figure 17. The peaks representing northwesterly and northeasterly winds at 11:44 and 11:55 in Figure 17 coincide with peaks polluted by MRFI from the north west and north east, in Figures 13 and 15. The horizontal wind vector, displayed in Figure 18, subjected to the MRFI removal algorithm shows reliable results, as the incorrectly calculated northwest wind and northeast wind series winds were removed, and the continuous wind vector is well restored with regard to time and altitude.

The above results suggest that MRFI can be sufficiently managed by software. Consequently, various costs can be reduced in considering environmental factors in equipment installation and operation. In addition, by using commonly used methods, researchers or users can easily apply them.

5. Conclusions

In the test operation stage of the wind profiler, we identified MRFI, a vertically discontinuous signal within a short altitude range. The MRFI occurred in multiple frequencies and was overlapping, unlike a general external RFI. We developed an algorithm to automatically remove MRFI from the spectrum stage for work-site operation. To the best of our knowledge, neither MRFI nor this algorithm have been reported in previous studies. The first step in the MRFI removal process is distinguishing between non-meteorological and meteorological signals and determining a threshold based on the spectrum width. The second step is to detect and remove the RFI according to its characteristics. Finally, the overlapping signals are removed using an iterative process. In order to prevent the meteorological signal from being removed in this process, we set the optimal criterion based on the number of gates obtained through several tests. In April 2021, the algorithm was validated to effectively remove MRFI, as well as general external RFI. Although tests were not performed at the IQ signal stage due to the lack of convenience of data utilization and the need for heavy memory capacity, the algorithm was qualitatively verified through continuity evaluation with a time series of spectra and wind vectors before and after the algorithm application. Notably, MRFI was effectively removed in the spectrum stage, and continuous wind vectors were restored by revised moment data. In the future, we intend to apply this algorithm to other wind profiler models for data quality control.

Author Contributions: Conceptualization, K.H.L. and B.H.K.; methodology, K.H.L.; software, K.H.L.; validation, K.H.L. and B.H.K.; formal analysis, K.H.L. and B.H.K.; investigation, K.H.L.; resources, K.H.L.; data curation, K.H.L.; writing—original draft preparation, K.H.L.; writing—review and editing, K.H.L. and B.H.K.; visualization, K.H.L.; supervision, B.H.K.; project administration, B.H.K.; funding acquisition, B.H.K. All authors have read and agreed to the published version of the manuscript.

Funding: This research was funded by the Defense Acquisition Program Administration and Korea Meteorological Administration, grant numbers 17-CM-SS-23 and KMA2017-04210, and ‘Development of fusion technology for Radar wind profiler’ and ‘Development of radar based severe weather monitoring technology,’ grant number KMA2021-03121, of the ‘Development of integrated application technology for Korea weather radar’ project funded by the Weather Radar Center, Korea Meteorological Administration.

Institutional Review Board Statement: Not applicable.

Informed Consent Statement: Not applicable.

Data Availability Statement: All resulting data are available upon request from Kyung Hun Lee (lee_buzz@nate.com). Software code and raw data are not available for the security reasons of government agencies.

Acknowledgments: This research has been supported by the Defense Acquisition Program Administration and the Korea Meteorological Administration and was conducted using the resources and facilities of Pukyong National University and the National Typhoon Center.

Conflicts of Interest: The authors declare no conflict of interest.

References

1. Brewster, K.A. *Profiler Training Manual # 2: Quality Control of Wind Profiler Data*; National Weather Service Office of Meteorology: Boulder, CO, USA, 1989.
2. Muradyan, P.; Coulter, R. *Radar Wind Profiler (RWP) and Radio Acoustic Sounding System (RASS) Instrument Handbook*; U.S. Department of Energy—Office of Science: Washington, DC, USA, 2020.
3. Chen, Z.; Chu, Y.; Su, C. Intercomparisons of Tropospheric Wind Velocities Measured by Multi-Frequency Wind Profilers and Rawinsonde. *Atmosphere* **2021**, *12*, 1284. [[CrossRef](#)]
4. Lau, E.; McLaughlin, S.; Pratte, F.; Weber, B.; Merritt, D.; Wise, M.; Zimmerman, G.; James, M.; Sloan, M. The DeTect Inc. RAPTOR VAD-BL Radar Wind Profiler. *J. Atmos. Ocean. Technol.* **2013**, *30*, 1978–1984. [[CrossRef](#)]
5. May, P.T.; Strauch, R.G. Reducing the Effect of Ground Clutter on Wind Profiler Velocity Measurements. *J. Atmos. Ocean. Technol.* **1998**, *15*, 579–586. [[CrossRef](#)]
6. Muschinski, A.; Lehmann, V.; Justen, L.; Teschke, G. Advanced Radar Wind Profiling. *Meteorol. Z.* **2005**, *14*, 609–625. [[CrossRef](#)]
7. Ai, W.; Huang, Y.; Hu, M.; Shen, C. Ground Clutter Removing for Wind Profiler Radar Signal Using Adaptive Wavelet Threshold. In Proceedings of the 2010 International Conference on Measuring Technology and Mechatronics Automation, Changsha, China, 13–14 March 2010. [[CrossRef](#)]
8. Williams, C.R.; Maahn, M.; Hardin, J.C.; de Boer, G. Clutter Mitigation, Multiple Peaks, and High-Order Spectral Moments in 35 GHz Vertically Pointing Radar Velocity Spectra. *Atmos. Meas. Tech.* **2018**, *11*, 4963–4980. [[CrossRef](#)]
9. Pekour, M.S. Removal of Bird Contamination in Wind Profiler Signal Spectra. In Proceedings of the 9th International Symposium on Acoustic Remote Sensing and Associated Techniques of the Atmosphere and Oceans, Vienna, Austria, 7 June–7 October 1998.
10. Kretzschmar, R.; Karayiannis, N.B.; Richner, H. Removal of Bird-Contaminated Wind Profiler Data Based on Neural Networks. *Pattern Recognit.* **2003**, *36*, 2699–2712. [[CrossRef](#)]
11. Jordan, J.; Leach, J.; Wolfe, D. Operation of a Mobile Wind Profiler in Severe Clutter Environments. In Proceedings of the 12th Symposium on Meteorological Observations and Instrumentation, American Meteorological Society, Long Beach, CA, USA, 8–13 February 2003.
12. Electronic Communications Committee (ECC) within the European Conference of Postal and Telecommunications Administrations (CEPT). *Compatibility of Wind Profiler Radars in the Radio Location Service (RLS) with the Radio Navigation Satellite Service (RNSS) in the Band 1270–1295 MHz*; ECC: Lübeck, Germany, 2006; Available online: <https://docdb.cept.org/download/411> (accessed on 7 January 2022).
13. Lehmann, V. Use of Radar Wind Profilers in Operational Networks. In Proceedings of the WMO Technical Conference (TECO) on Meteorological and Environmental Instruments and Methods of Observation, Helsinki, Finland, 30 August–1 September 2010.
14. Bollian, T.; Osmanoglu, B.; Rincon, R.F.; Lee, S.; Fatoyinbo, T. MVDR Beamforming for RFI Suppression in EcoSAR Data. In Proceedings of the EUSAR 2018: 12th European Conference on Synthetic Aperture Radar, Aachen, Germany, 4–7 June 2018.
15. Tao, M.; Su, J.; Huang, Y.; Wang, L. Mitigation of Radio Frequency Interference in Synthetic Aperture Radar Data: Current Status and Future Trends. *Remote Sens.* **2019**, *11*, 2438. [[CrossRef](#)]
16. Emery, B.; Camps, A. *Introduction to Satellite Remote Sensing: Atmosphere, Ocean, Land and Cryosphere Applications*; Elsevier: Amsterdam, The Netherlands, 2017.
17. Wilczak, J.M.; Strauch, R.G.; Ralph, F.M.; Weber, B.L.; Merritt, D.A.; Jordan, J.R.; Wolfe, D.E.; Lewis, L.K.; Wuertz, D.B.; Gaynor, J.E.; et al. Contamination of Wind Profiler Data by Migrating Birds: Characteristics of Corrupted Data and Potential Solutions. *J. Atmos. Ocean. Technol.* **1995**, *12*, 449–467. [[CrossRef](#)]
18. Lambert, W.C.; Merceret, F.J.; Taylor, G.E.; Ward, J.G. Performance of Five 915-MHz Wind Profilers and an Associated Automated Quality Control Algorithm in an Operational Environment. *J. Atmos. Ocean. Technol.* **2003**, *20*, 1488–1495. [[CrossRef](#)]
19. Weber, B.L.; Wuertz, D.B. *Quality Control Algorithm for Profiler Measurements of Winds and Temperatures*; Wave Propagation Laboratory: Boulder, CO, USA, 1991.
20. Weber, B.L.; Wuertz, D.B.; Welsh, D.C.; McPeck, R. Quality Controls for Profiler Measurements of Winds and RASS Temperatures. *J. Atmos. Ocean. Technol.* **1993**, *10*, 452–464. [[CrossRef](#)]
21. Griesser, T.; Richner, H. Multiple Peak Processing Algorithm for Identification of Atmospheric Signals in Doppler Radar Wind Profiler Spectra. *Meteorol. Z.* **1998**, *7*, 292–302. [[CrossRef](#)]
22. Wolfe, D.; Weber, B.; Wilfong, T.; Welsh, D.; Wuertz, D.; Merritt, D. NOAA Advanced Signal Processing System for Radar Wind Profilers. In Proceedings of the 11th Symposium on Meteorological Observations and Instrumentation, Albuquerque, NM, USA, 14–18 January 2001.
23. Morse, C.S.; Goodrich, R.K.; Cornman, L.B. The NIMA Method for Improved Moment Estimation from Doppler Spectra. *J. Atmos. Ocean. Technol.* **2002**, *19*, 274–295. [[CrossRef](#)]

24. Lehmann, V.; Teschke, G. Advanced Intermittent Clutter Filtering for Radar Wind Profiler: Signal Separation through a Gabor Frame Expansion and Its Statistics. *Ann. Geophys.* **2008**, *26*, 759–783. [[CrossRef](#)]
25. Lehmann, V.; Teschke, G. Wavelet Based Methods for Improved Wind Profiler Signal Processing. *Ann. Geophys.* **2001**, *19*, 825–836. [[CrossRef](#)]
26. Lehtinen, R.; Jordan, J. Improving Wind Profiler Measurements Exhibiting Clutter Contamination Using Wavelet Transforms. In Proceedings of the WMO Technical Conference on Meteorological and Environmental Instruments and Methods of Observation (TECO-2006), Geneva, Switzerland, 4–6 December 2006.
27. Kim, M.; Kim, K.; Kim, P.; Kang, D.; Kwon, B.H. Local Wind Field Simulation over Coastal Areas Using Windprofiler Data. *J. Korean Soc. Mar. Environ. Saf.* **2016**, *22*, 195–204. [[CrossRef](#)]
28. Van de Kamp, D.W. *Profiler Training Manual # 1: Principles of Wind Profiler Operation*; National Weather Service Office of Meteorology: Boulder, CO, USA, 1989.
29. World Meteorological Organization (WMO). *Guide to Meteorological Instruments and Methods of Observation*, 2008 ed.; WMO: Geneva, Switzerland, 2008; Volume 2010.
30. Jordan, J.R.; Lataitis, R.J.; Carter, D.A. Removing Ground and Intermittent Clutter Contamination from Wind Profiler Signals Using Wavelet Transforms. *J. Atmos. Ocean. Technol.* **1997**, *14*, 1280–1297. [[CrossRef](#)]
31. Barbré, R., Jr. Development of a climatology of vertically complete wind profiles from Doppler Radar Wind Profiler systems. In Proceedings of the American Meteorological Society (AMS) Conference on Aviation, Range and Aerospace Meteorology (ARAM), Phoenix, AZ, USA, 4–8 January 2015.
32. Cornman, L.B.; Goodrich, R.K.; Morse, C.S.; Ecklund, W.L. A Fuzzy Logic Method for Improved Moment Estimation from Doppler Spectra. *J. Atmos. Ocean. Technol.* **1998**, *15*, 1287–1305. [[CrossRef](#)]
33. Bianco, L.; Wilczak, J.M. Convective Boundary Layer Depth: Improved Measurement by Doppler Radar Wind Profiler Using Fuzzy Logic Methods. *J. Atmos. Ocean. Technol.* **2002**, *19*, 1745–1758. [[CrossRef](#)]
34. Allabakash, S.; Yasodha, P.; Bianco, L.; Reddy, S.V.; Srinivasulu, P. Improved Moments Estimation for VHF Active Phased Array Radar Using Fuzzy Logic Method. *J. Atmos. Ocean. Technol.* **2015**, *32*, 1004–1014. [[CrossRef](#)]
35. Sinha, S.; Lourde, R.M.; Sarma, T.V.C. An Efficient Method of RFI and Clutter Removal in Wind Profiler Spectra. In Proceedings of the 2016 IEEE 59th International Midwest Symposium on Circuits and Systems (MWSCAS), Abu Dhabi, United Arab Emirates, 16–19 October 2016. [[CrossRef](#)]
36. Hildebrand, P.H.; Sekhon, R.S. Objective Determination of the Noise Level in Doppler Spectra. *J. Appl. Meteorol.* **1974**, *13*, 808–811. [[CrossRef](#)]
37. Kim, H.; Jang, M.; Lee, E. Meteor-Statistical Analysis for Establishment of Jeju Wind Resource Database. *J. Environ. Sci.* **2008**, *17*, 591–599. (In Korean) [[CrossRef](#)]
38. Yoon, H.; Jang, B. Frequency Interference, Analysis Method, and Application Examples of Sub-GHz Frequency Band. *J. Korean Inst. Electromagn. Eng. Sci.* **2021**, *32*, 1–9. (In Korean) [[CrossRef](#)]
39. ISO/DIS 23032(en); Meteorology—Ground-Based Remote Sensing of Wind—Radar Wind Profiler. ISO: Geneva, Switzerland, 2022. Available online: <https://dgn.isolutions.iso.org/obp/ui#iso:std:iso:23032:dis:ed-1:v1:en> (accessed on 6 January 2022).
40. Nguyen, L.H.; Tran, T.D. Estimation and Extraction of Radio-Frequency Interference from Ultra-Wideband Radar Signals. In Proceedings of the 2015 IEEE International Geoscience and Remote Sensing Symposium (IGARSS), Milan, Italy, 26–31 July 2015. [[CrossRef](#)]
41. The Right Radar Wind Profiler for Your Application. Available online: https://library.wmo.int/pmb_ged/iom_116_en/Session%201/O1_9_McLaughlin_RightRWPforJob.pdf (accessed on 7 January 2022).
42. Zhongming, Z.; Linong, L.; Xiaona, Y.; Wangqiang, Z.; Wei, L. *Experience of the Japan Meteorological Agency with the Operation of Wind Profilers*; World Meteorological Organization (WMO): Geneva, Switzerland, 2012; Volume 110.
43. Strauch, R.G.; Merritt, D.A.; Moran, K.P.; Earnshaw, K.B.; De Kamp, D.V. The Colorado Wind-Profiling Network. *J. Atmos. Ocean. Technol.* **1984**, *1*, 37–49. [[CrossRef](#)]

Disclaimer/Publisher’s Note: The statements, opinions and data contained in all publications are solely those of the individual author(s) and contributor(s) and not of MDPI and/or the editor(s). MDPI and/or the editor(s) disclaim responsibility for any injury to people or property resulting from any ideas, methods, instructions or products referred to in the content.